

PAPER • OPEN ACCESS

## A neurostimulator system for real, sham, and multi-target transcranial magnetic stimulation

To cite this article: Majid Memarian Sorkhabi and Timothy Denison 2022 *J. Neural Eng.* **19** 026035

View the [article online](#) for updates and enhancements.

### You may also like

- [Effective electric fields along realistic DTI-based neural trajectories for modelling the stimulation mechanisms of TMS](#)  
N De Geeter, G Crevecoeur, A Leemans et al.
- [Coil model comparison for cerebellar transcranial magnetic stimulation](#)  
M Kaan Çan, Ilkka Laakso, Jaakko O Nieminen et al.
- [A multichannel magnetic stimulation system using submillimeter-sized coils: system development and experimental application to rodent brain \*in vivo\*](#)  
Shunsuke Minusa, Shuto Muramatsu, Hisayuki Osanai et al.



## PAPER

## OPEN ACCESS

## RECEIVED

23 November 2021

## REVISED

21 March 2022

## ACCEPTED FOR PUBLICATION

24 March 2022

## PUBLISHED

12 April 2022

Original content from this work may be used under the terms of the [Creative Commons Attribution 4.0 licence](#).

Any further distribution of this work must maintain attribution to the author(s) and the title of the work, journal citation and DOI.



# A neurostimulator system for real, sham, and multi-target transcranial magnetic stimulation

Majid Memarian Sorkhabi<sup>1,\*</sup>  and Timothy Denison<sup>1,2</sup><sup>1</sup> MRC Brain Network Dynamics Unit, Nuffield Department of Clinical Neurosciences, University of Oxford, Oxford OX1 3TH, United Kingdom<sup>2</sup> Department of Engineering Science, University of Oxford, Oxford OX1 3PJ, United Kingdom

\* Author to whom any correspondence should be addressed.

E-mail: [majid.memariansorkhabi@ndcn.ox.ac.uk](mailto:majid.memariansorkhabi@ndcn.ox.ac.uk)**Keywords:** transcranial magnetic stimulation, TMS, TMS pulse generator, sham stimulation, multi-target stimulation, brain stimulationSupplementary material for this article is available [online](#)

## Abstract

**Objective.** Transcranial magnetic stimulation (TMS) is a clinically effective therapeutic instrument used to modulate neural activity. Despite three decades of research, two challenging issues remain, the possibility of changing the (a) stimulated spot and (b) stimulation type (real or sham) without physically moving the coil. In this study, a second-generation programmable TMS device with advanced stimulus shaping is introduced that uses a five-level cascaded H-bridge inverter and phase-shifted pulse-width modulation. The principal idea of this research is to obtain real, sham, and multi-locus stimulation using the same TMS system. **Approach.** We propose a two-channel modulation-based magnetic pulse generator and a novel coil arrangement, consisting of two circular coils with a physical distance of 20 mm between the coils and a control method for modifying the effective stimulus intensity, which leads to the live steerability of the target and type of stimulation. **Main results.** Based on the measured system performance, the stimulation profile can be steered  $\pm 20$  mm along a line from the centroid of the coil locations by modifying the modulation index. **Significance.** The proposed system supports electronic control of the stimulation spot without physical coil movement, resulting in tunable modulation of targets, which is a crucial step towards automated TMS machines.

## 1. Introduction

Transcranial magnetic stimulation (TMS) is a non-invasive technique used to stimulate and modulate cortical neurons [1, 2]. TMS is based on the fundamental principles of electromagnetic induction: a brief, strong electric current is delivered to the windings of a coil, inducing a changing magnetic field, which in turn induces an electric field (E-field) in the cortex. Applying magnetic stimulation to neural cells can depolarize and hyperpolarize neurons. TMS is commonly used as a diagnostic tool for various neurological disorders; it is an FDA-approved treatment of, for example, major depressive disorder, and is being considered as a potential therapy for many other applications [2, 3].

Conventional magnetic stimulators consist of three main elements: a power capacitor, an inductor

acting as the stimulation coil, and a thyristor switch to control the connection between them [4]. Most stimulators are restricted to specific stimulus frequencies and shapes, generating only monophasic or biphasic cosine-shaped pulses. Typically, the stimulus frequency is approximately 2.5 kHz, but the exact value is determined by the architecture of the stimulator and the coil. During biphasic stimulation, some of the energy delivered by the pulse is recovered, enabling the generation of up to 100 pulses  $s^{-1}$  [5]. However, in monophasic stimulation, the energy is dissipated through a resistor [4], only allowing stimulation patterns of one pulse per second at full power.

The ancillary effects of TMS, such as clicking noise, stimulation of nearby peripheral nerves, and scalp and facial sensations may interfere with task performance in clinical research through subject biasing and distraction, which can contaminate trial

outcomes [6, 7]. Subjects in the control group, who were exposed to all artifacts but did not receive stimulation in the target brain area, could help to separate the effects of the auditory and tactile artifacts from the test group. Physically tilting the coil from  $45^\circ$  to  $90^\circ$  from the target brain area, electrical scalp stimulation during the sham TMS [8], flipping the current direction in each of the Figure-of-eight coils by an external custom-made switch box or changing the direction of the winding inside the coil, are examples of conventional methods for implementing a sham-TMS protocol [9, 10].

Another constraint is maintaining the target location of the stimulation, which is a considerable challenge of the TMS technique. Neuro-navigation technology can sustain the target in a couple of millimeters using robotic arms and physical coil displacement [11]. In addition to the high cost and complexity of these systems, the safe handling of heavy coils is relatively slow, and it is practically impossible to move the target location during rapid stimulation protocols. Using an array of coils, such as a 16-coil or 5-coil, can theoretically solve the problem of moving the target location, but a separate TMS system is required to drive each coil [12]. In addition to being bulky and expensive systems, the dynamics of conventional pulse generators will probably not allow the stimulus parameters to be modified quickly enough for repetitive protocols. The multi-locus TMS system introduced by Koponen *et al* [12], which consists of an optimized figure-of-eight coil and an oval coil stacked on top of each other, can move the stimulated spot in a  $\pm 15$  mm long line from the coil center, which has certain limitations in terms of the speed of spot movement and stimulus generation for rapid TMS protocols.

Navarro de Lara *et al* introduced a 3-axis coil design to enable multiple cortex locations to be stimulated without physical coil movement [13]. The  $x/y$  direction coils were wound on a spherical coil form, and the  $z$ -direction coil was a circular type coil parallel to a skull. The pulse generator used in that design was a modified biphasic resonant-based circuit with two output channels. Although their design allowed flexible spatiotemporal E-field control, a delay of stimulus polarity inversion may limit the field control for rotating field protocols.

Recently, the use of isolated-gate bipolar transistors (IGBTs) instead of thyristors, as well as the implementation of H-bridge structures, has enabled more control over the stimulation parameters. Peterchev *et al* developed a series of transcranial magnetic stimulators with controllable pulse parameters (cTMS) [14–16] that produce both monophasic and biphasic stimuli of different frequencies and allow more pulses per second than conventional TMS devices. However, the high current stress on the IGBTs and the limited

number of pulses that can be selected limit the achievable protocols [17].

A new approach using pulse width modulation (PWM) enables the imitation of any arbitrary stimulus while reducing the current stress on the IGBTs, called programmable TMS (pTMS) [17]. This structure can reduce the current stress on the power switches by paralleling IGBTs. Also, by recovering the energy delivered to the coil, the proposed design can generate magnetic pulses with a high repetition rate (up to 1 kHz), low interstimulus intervals (1 ms), and low voltage decay.

Morphological models of neurons and preliminary results of in-human experiments reveal that the conventional monophasic and its PWM equivalent pulses can induce relatively identical results on the primary motor cortex, and the PWM stimuli appear to fundamentally approximate the effect of conventional magnetic pulses [18, 19].

Nowadays, power converter technology has been applied in many fields, such as motor drivers, electric vehicles, renewable energy sources, and magnetic resonance imaging (MRI) scanners. Among power converter methods, multilevel inverter topologies, including cascaded H-bridges (CHBs), flying capacitors, and modular multilevel converters, are industrially accepted solutions for medium-voltage high-power applications. Broadly, the CHB architecture has received more attention because of its simple layout and construction, high modularity, uncomplicated control of power switches, the need for fewer power switches, and no voltage balance problems in energy storage capacitors. These features make CHB inverters a convenient solution to be applied as a TMS pulse generator core.

This study introduces the second generation of a pTMS device that uses these advantages to generate arbitrary stimulus shapes via the PWM technique. For this purpose, we describe how  $N$  H-bridge cells could be cascaded to reach PWM pulses with  $(2N + 1)$  voltage levels. Also, how to generate control signals of IGBTs for cascaded  $N$  cells. We propose the use of the modulation index concept to steer the stimulation locus, which is a feasible solution to the problem of delay in charging and discharging pulse capacitors for multichannel TMS designs. Also, the proportional-integral (PI) control loop is introduced here for the first time in TMS devices to minimize the current distortions.

This research also aims to develop a versatile TMS system, including a pulse generator and a novel coil arrangement, to control the stimulation type and location. The concept of modulation index and the control of effective stimulus intensity in each of the coils play a major role in this goal. To measure the performance of the proposed system, we built a two-channel pTMS device and two non-overlapping circular coils.

## 2. Materials and methods

### 2.1. Coil design

A custom-made figure-of-eight coil with two loops of 70 mm-diameter circular coils was designed and manufactured, where the distance from the edge to the edge of the two coils was 20 mm, and each of the two wings was controlled separately (Magstim Company Ltd, UK). Both coils were placed individually in a coil enclosure. The coils were air-cooled and had four independent temperature monitoring points on the coils. The left and right coil inductances were measured at 18  $\mu\text{H}$  and 18.3  $\mu\text{H}$ , respectively, and because of the physical distance between the coils, their mutual inductance can be neglected. More details are available in the appendix (figure A1 available online at [stacks.iop.org/JNE/19/026035/mmedia](https://stacks.iop.org/JNE/19/026035/mmedia)).

Electromagnetic simulations were performed using COMSOL software (V5.3, Sweden) with the finite element method (FEM), using the AC/DC module. A 3D MRI-derived head model was used to calculate the induced E-field. The head tissue was assumed to be homogeneous, with an electrical conductivity of  $\sigma = 0.333 \text{ S m}^{-1}$  [20]. For the FEM analysis, the final mesh structure of the coil and head comprised 145 000 nodes and 3.1 million tetrahedral elements, with a minimum element size of 5  $\mu\text{m}$ . A linear solver with a relative error of  $1.2 \times 10^{-6}$  was selected. During the FEM simulation, the coil and head models were placed in the air.

To validate the modeling results and estimate the accuracy of the pulse generator and the manufactured coil, a custom system with a pickup coil was designed that swept the  $40 \times 50 \text{ mm}$  area with 5 mm steps and measured the induced E-field.

### 2.2. Magnetic pulse generator

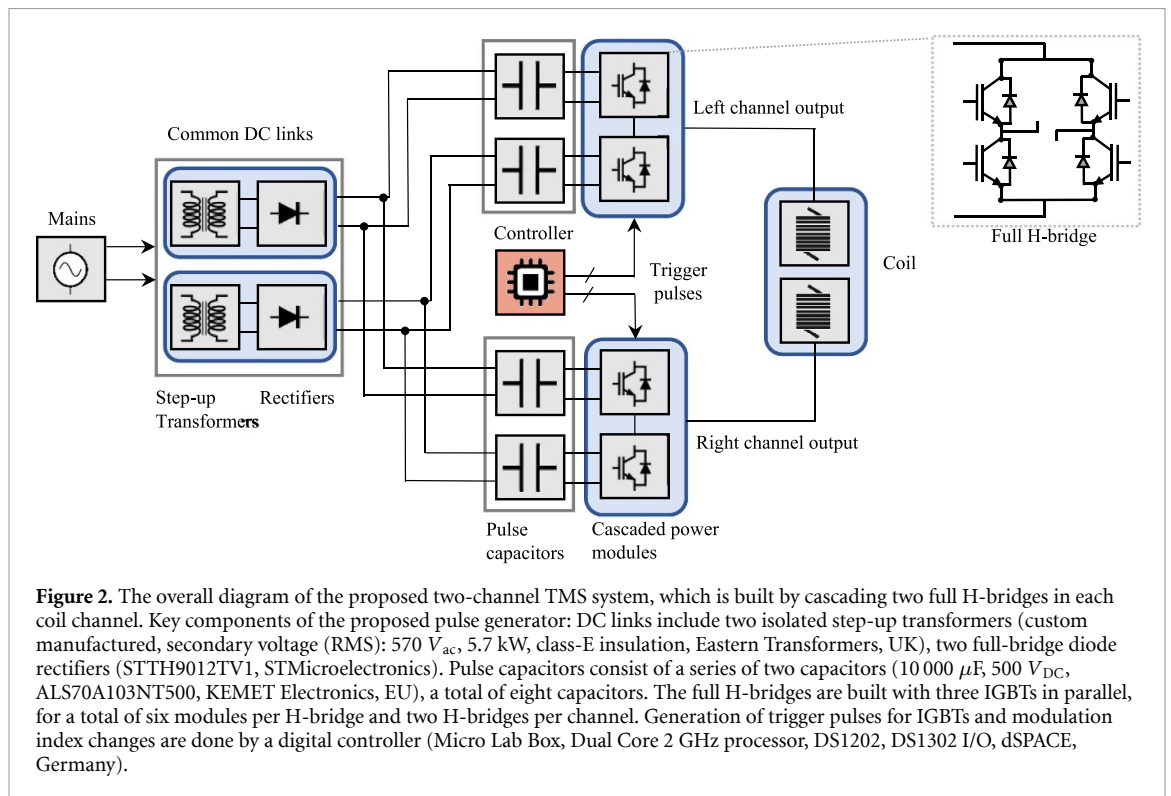
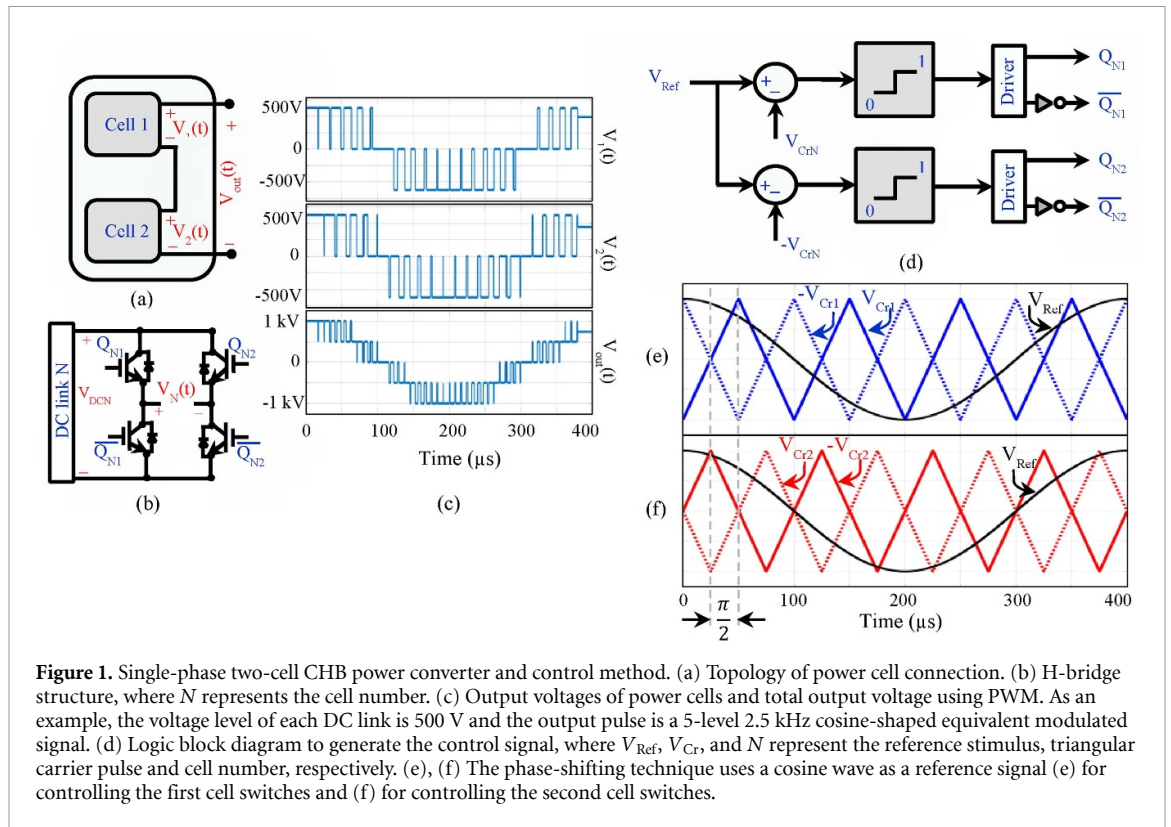
As shown in figure 1, the CHB inverter consists of a series of  $N$  power cells, usually based on identical H-bridge sub-modules that are cascaded from the cell output. Each of them includes a galvanically isolated DC link as a voltage source and an energy storage capacitor. If the DC link voltage is equal in all the cells, CHB is classified as a symmetric inverter, but if the voltages of each power cell are dissimilar, it is classified as an asymmetric architecture. Although an asymmetric CHB with a smaller number of power cells can generate a greater voltage level, controlling the returning (regenerative) currents from inductive loads, such as stimulation coils in TMS devices, and maintaining capacitor voltage balance can be challenging. In addition, modularity and lower implementation and maintenance costs are other advantages of a symmetrical CHB over an asymmetric inverter [21]. In this study, a symmetrical structure was selected and implemented. Each H-bridge can be used to create three output voltage levels:  $\{-V_{\text{DC}}, 0, +V_{\text{DC}}\}$ . Thus,

by connecting two cells, five voltage levels  $\{-2V_{\text{DC}}, -V_{\text{DC}}, 0, +V_{\text{DC}}, +2V_{\text{DC}}\}$  can be achieved for the output pulse. As represented in figure 1(c), the output voltages of the H-bridges ( $V_1(t)$  and  $V_2(t)$ ) are similar but displaced in time, and the total output pulse ( $V_{\text{out}}(t)$ ) is the sum of the outputs of the two cells.

For a multilevel inverter, multicarrier phase-shifted PWM (PS-PWM) is a common method for creating the switching pulses of power devices [22, 23] introduced in figure 1(d). In PS-PWM, triangular carrier pulses ( $V_{\text{cr}}$ ) with the same frequency but shifted by a specific phase are compared with the desired reference signal ( $V_{\text{Ref}}$ ) to determine the trigger signal for the power switches ( $Q_{N1}, \overline{Q_{N1}}, Q_{N2}, \overline{Q_{N2}}$ ). The carriers are shifted by  $\pi/N$  rad, where  $N$  is the total number of H-bridges. Figures 1(d)–(f) shows the PS-PWM method for the structure implemented in this study, a two-cell CHB inverter where carriers have a phase difference of  $\pi/2$  rad [24, 25].

The PS-PWM method has a multiplicative effect on switching frequency. While each cell can be triggered at a low switching frequency, the final output pulse is the sum of the output voltages of the cells ( $V_1(t) + V_2(t) = V_{\text{out}}(t)$ ) and its harmonic components will be at higher frequencies than the output of each cell [26]. As an example, if the PS-PWM technique is employed in an  $N$ -cell CHB and the triangular carrier frequencies are  $F_{\text{PWM}}$ , due to the switching, the first harmonic in the output voltage ( $V_{\text{out}}(t)$ ) will be located at  $N \cdot 2 \cdot F_{\text{PWM}}$  [24, 27]. This feature makes the CHB inverter very attractive for TMS pulse generators. Because the inherent low-frequency property of the neural tissue is expected to attenuate the high-frequency harmonics produced by switching, the neurons would only respond to the main harmonic component, which is the reference pulse frequency.

In this study, a dedicated two-channel TMS device was used to generate magnetic stimuli. For this purpose, for each coil channel, two full H-bridges are cascaded together, which can generate 5-level PWM pulses, as shown in figure 2. The pulse capacitors of each H-bridge are implemented separately, but two isolated DC sources (including step-up transformers and rectifiers) and the controller are commonly used for both channels. The proposed coil can be also connected to two individual systems and by generating synchronous pulses, the stimulation site can be shifted, or the stimulation type can be changed (real or sham). If a dedicated two channel TMS system is used, some of the required components can be shared, as shown in figure 2. The dedicated multichannel system would reduce overall costs and cut the size of the device, especially if a large-scale multichannel system is required with more coils in future works. The controller used here (Micro Lab Box, dSPACE, Germany), can trigger up to 12 individual pTMS systems.



If more devices need to be run synchronously for large-scale systems, the number of controllers should be increased. Depending on the desired stimulation protocol and the number of H-bridges connected to the common DC link, scaling considerations such as

power electronics and step-up transformers would need consideration.

In power-electronic systems, existing semiconductor switches are one of the most fragile items that could fail under the immense current stress



associated with pulsed-powered applications, such as TMS. Parallel-connected IGBTs break the problem of simultaneous high coil current demand into smaller, manageable portions, distributed across several relatively identical switches and effectively mitigate the current stress on IGBTs [28]. In this work, three IGBT modules per leg were paralleled ( $V_{CEmax} = 1.2$  kV,  $I_{CRM} = 1.8$  kA, SEMiX603GB12E4p Semikron, Germany).

Variations of the manufacturing process may cause tolerances in IGBT specifications such as an internal stray inductance. Also, the parasitic inductance of the circuit can multiply asymmetric current sharing between parallel-connected IGBT modules. To mitigate this issue, low-ohmic-value resistors (500 m $\Omega$ , AP821R5J, Arco, UK) were added between the emitters and the driver to encourage the current sharing between IGBTs. These resistors act as negative feedback [29].

The DC link voltage is 1.5 kV (750 V per H-bridge) and the measured peak current for the 2.5 kHz biphasic pulse is 6 kA.

### 2.3. PI controller design

The PI control loop mechanism is utilized in the CHB inverter control feedback, where the reference coil current is defined as the desired set point for the minimization of current distortions [30]. Parasitic resistance loss in the coil and switching losses of IGBTs are the main causes of these distortions in the TMS system, which can be minimized by optimizing the PWM patterns. This optimization method was calculated offline, and a look-up table that holds the trigger pulses was generated. The content of this look-up table is a function of the desired stimulus waveforms and treatment procedures. Offline computation was performed by modeling and reconstructing the circuit behavior by utilizing the commutated current, voltage, and semiconductor characteristics. Finally, the controller parameters were tuned using a laboratory testbed. Moreover, the safe operating limits of the TMS machine were added to the controller design formulation. Even more imperative, for the PI controller, a significant part of the control effort is shifted from the hardware stage to the computational stage.

The feedback PI control system is shown in figure 3(a), where  $I^*(s)$ ,  $E(s)$ ,  $U(s)$ ,  $T(s)$ , and  $I(s)$  denote the Laplace transforms of the reference current signal, error signal, control signal, switching actions and actual current of inverter respectively. For the PI controller,  $P$  is the proportional gain and  $I$  is the integral gain. The aim is to design a controller that manipulates the IGBTs in the inverter that the coil current  $I(s)$  closely tracks its reference  $I^*(s)$ .

#### 2.3.1. Performance evaluation of PI controller

In the following, simulation results are provided to demonstrate the performance of the PI controller

with reference tracking. The load has the inductance  $L = 15.5$   $\mu$ H and the parasitic resistance  $R = 35$  m $\Omega$  (typical figure-8 coil). Under steady-state operating conditions, the reference current signal is a sinusoidal waveform with the fundamental frequency of 2.5 kHz (typical biphasic magnetic stimulus), the inverter is a two-cell CHB with five-level PWM pulses, three parallel-IGBTs per leg, and the IGBT on-resistance is  $r_{CE} = 2$  m $\Omega$ . For the modulation block: multicarrier PS-PWM is used with  $F_{PWM} = 4$  kHz.

The first scenario is bypassing the PI controller from the feedback loop. As shown in figure 3(b), there is a significant difference between the coil current and the reference current. The resulting total harmonic distortion (THD) of the current is  $I_{THD} = 17.2\%$ . In the second scenario, only the  $P$  controller is used in the loop ( $P = 1.75 \times 10^{-3}$ ) in this case, the THD will be reduced to  $I_{THD} = 11.47\%$ , as shown in figure 3(c). Finally, using the PI controller ( $P = 1.75 \times 10^{-3}$ ,  $I = 0.5 \times 10^{-3}$ ), the THD value is very small at  $I_{THD} = 4.52\%$ , and the coil current tracks its reference closely with a small current ripple. Figure 3(d) highlights the performance of the PI controller. To further lower the  $I_{THD}$ , the number of CHBs must be increased, although the filtering behavior of the neuronal membrane, when exposed to electromagnetic waves, causes the net effect of the applied pulse on the neuron to be a filtered pulse with a cut-off frequency of approximately 1 kHz [14]. Therefore, the applied staircase PWM pulses, which have high-frequency harmonics ( $I_{THD} \neq 0$ ), are observed as a softened pulse in the neuron.

### 2.4. Amplitude modulation index

The constant DC voltage in pulse capacitors and applied stimulation intensity alternation using the idea of amplitude modulation index ( $m$ ) greatly reduce the design complexity of AC to DC converters. This concept in multilevel inverters controls the effective intensity of the output pulse and provides an instant flexibility of the stimulation type and location by changing the pulse waveform. The modulation index, also known as the amplitude modulation ratio, is the ratio of the target pulse amplitude to the carrier signal amplitude, which is adjustable in the controller [31]. The CHB can produce an average output voltage that is linearly proportional to the target wave in the range of  $-1 \leq m \leq 1$  [17]. Potential distortions are minimized with the PI controller as a result of using this concept to control the effective stimulation intensity [32].

## 3. Results

Figure 4 shows the computational results for the induced E-field 20 mm below the coils, as the hypothetical location of the cortex, for the Magstim 70 mm Figure-of-eight coil (P/N 3190, figure 4(a)) and the proposed coil (figure 4(b)). The E-field profile for real

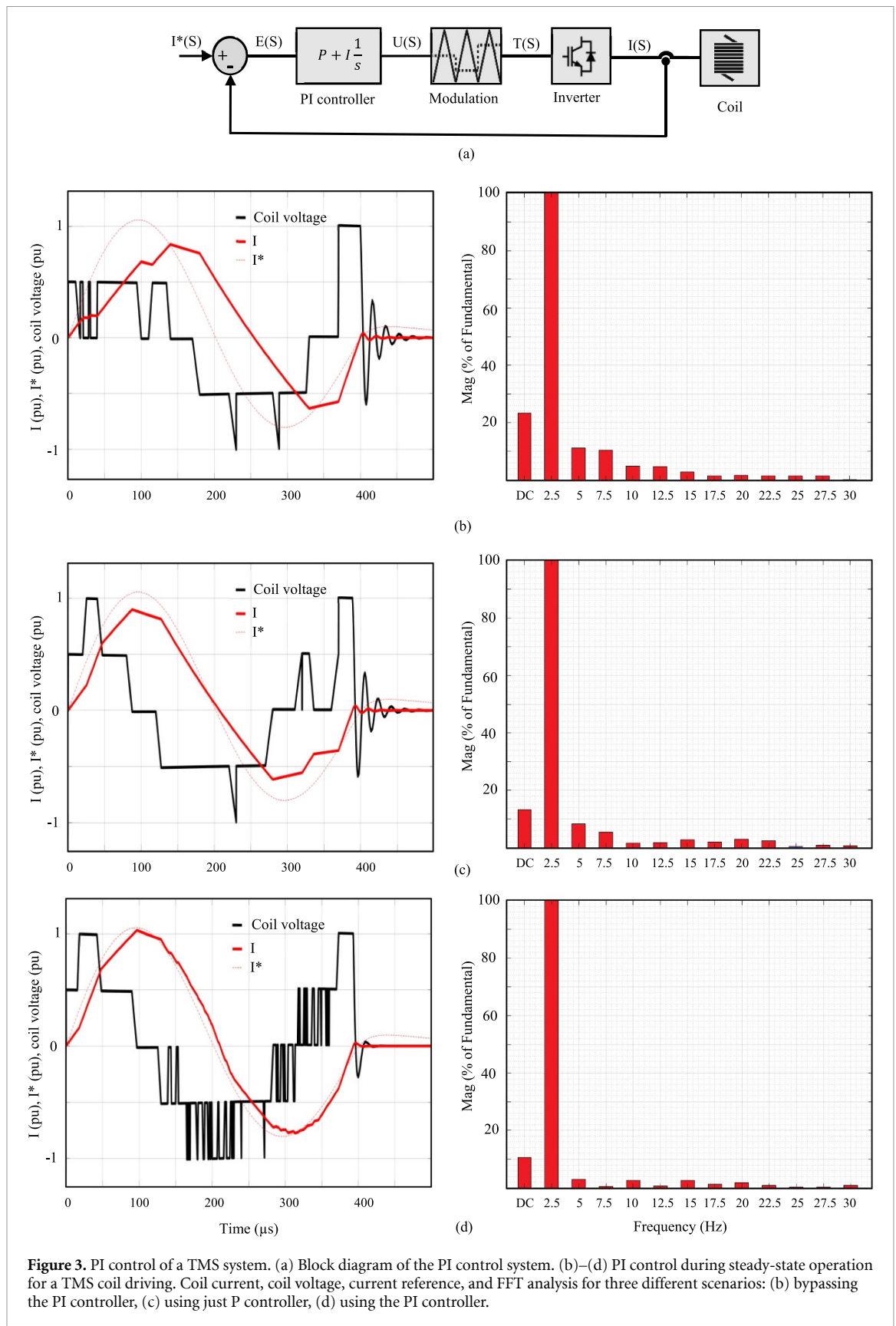


**Figure 3.** PI control of a TMS system. (a) Block diagram of the PI control system. (b)–(d) PI control during steady-state operation for a TMS coil driving. Coil current, coil voltage, current reference, and FFT analysis for three different scenarios: (b) bypassing the PI controller, (c) using just P controller, (d) using the PI controller.

stimulations is similar for the proposed and Figure-of-eight coils, and the difference is in the lower field concentration at the overlap area.

For the sham stimulation (figure 4(c)), it is obvious that in the central region, the E-fields of the

two coils attenuate each other and no stimulation will occur, but in areas below the coils, it is possible to see the stimulation. This off-target stimulation can lead to a sensation of stimulation in the subject and potentially make the placebo effect more

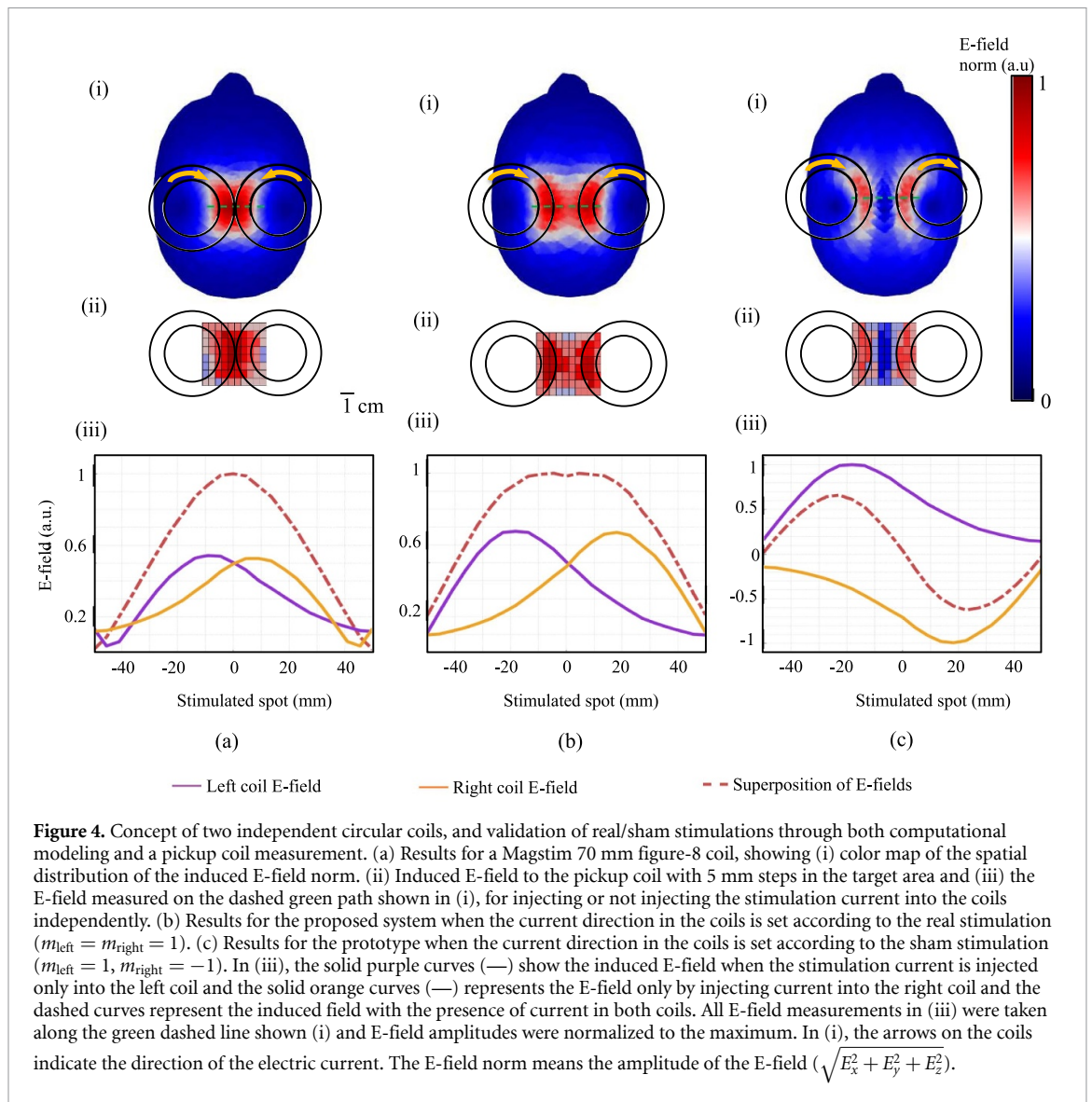


**Figure 4.** Concept of two independent circular coils, and validation of real/sham stimulations through both computational modeling and a pickup coil measurement. (a) Results for a Magstim 70 mm figure-8 coil, showing (i) color map of the spatial distribution of the induced E-field norm. (ii) Induced E-field to the pickup coil with 5 mm steps in the target area and (iii) the E-field measured on the dashed green path shown in (i), for injecting or not injecting the stimulation current into the coils independently. (b) Results for the proposed system when the current direction in the coils is set according to the real stimulation ( $m_{\text{left}} = m_{\text{right}} = 1$ ). (c) Results for the prototype when the current direction in the coils is set according to the sham stimulation ( $m_{\text{left}} = 1, m_{\text{right}} = -1$ ). In (iii), the solid purple curves (—) show the induced E-field when the stimulation current is injected only into the left coil and the solid orange curves (—) represents the E-field only by injecting current into the right coil and the dashed curves represent the induced field with the presence of current in both coils. All E-field measurements in (iii) were taken along the green dashed line shown (i) and E-field amplitudes were normalized to the maximum. In (i), the arrows on the coils indicate the direction of the electric current. The E-field norm means the amplitude of the E-field ( $\sqrt{E_x^2 + E_y^2 + E_z^2}$ ).

realistic. Measurements of sound pressure level for the same pulse intensities were not statistically different between the real and sham stimulation ( $\sim 70$  dB at 80% of the maximum device output,  $p = 0.45$ ).

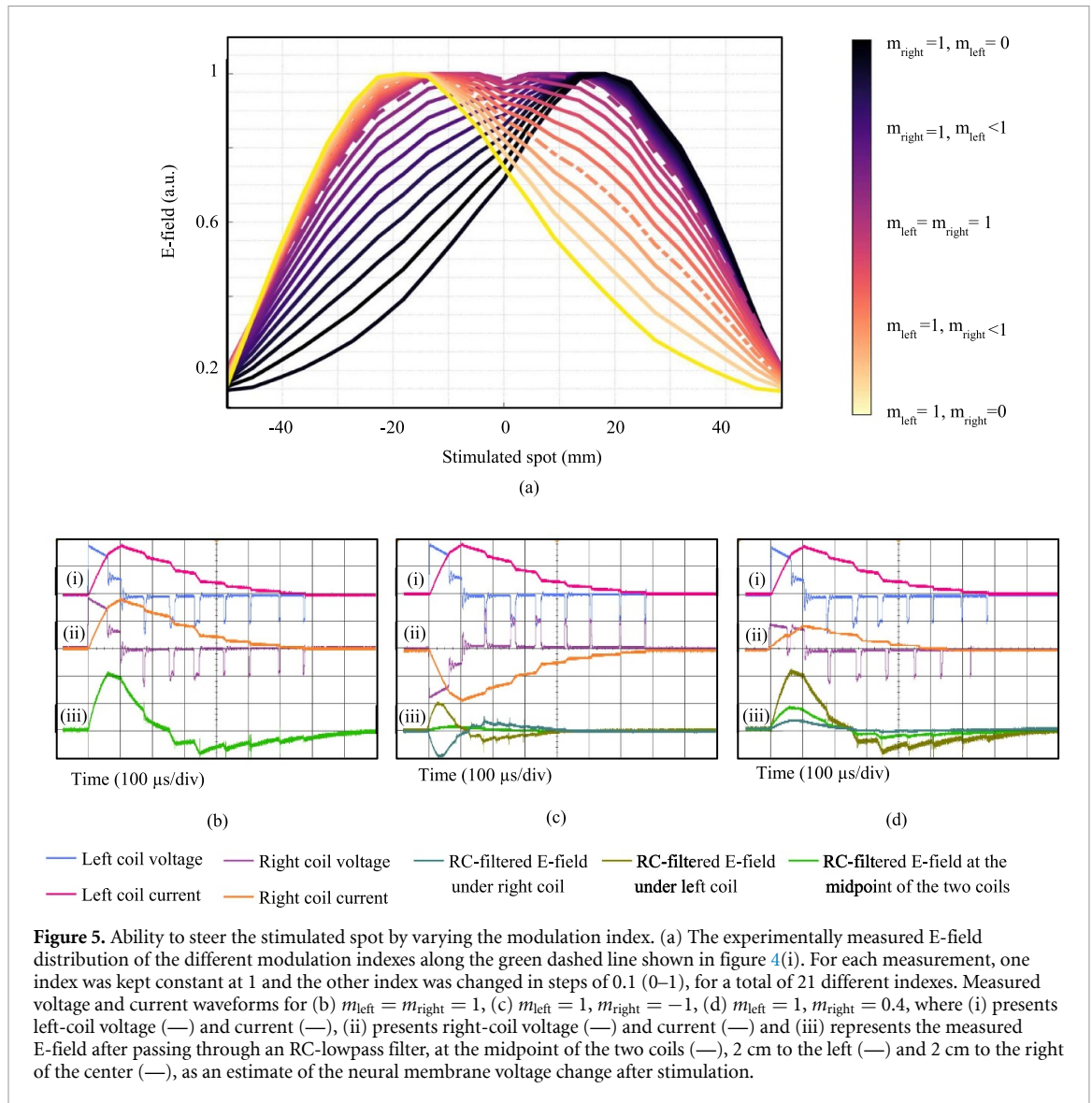
The results of the pickup coil measurements are shown in figure 4(ii). To investigate the effect of each coil loop on the final E-field profile, the coils were driven separately, and the peak E-fields were measured, as shown in figure 4(iii). Based on the results, the final stimulating field is the sum of the fields from each coil; therefore, by appropriately modifying the effective pulse intensity (modulation index), the induced E-field can be shaped and targeted without physical movement of the coils themselves.

To compare the measured E-field intensities against computational modeling from electromagnetic simulation, the E-field was evaluated at 20 mm from the bottom of the coils using a pickup coil. The measured maximum E-field norm for conventional figure-8 coil and two independent circular coils

were 197 and 193  $\text{V m}^{-1}$ , respectively. The maximum E-field values quantified by the modeling were 191  $\text{V m}^{-1}$  for the figure-8, and 188  $\text{V m}^{-1}$  for the two independent coils. The source of this error might be the accuracy of a calibrated high-voltage differential probe that we used to measure the voltage of the pulse capacitors and coils (TA044, PICO TECHNOLOGY, UK) and adjust the stimulus intensity, which is  $\pm 2\%$ . Therefore, it can be concluded that the performance of the implemented system is similar to that of the FEM modeling.

The physical translation of the stimulated spot while holding the locations of the coils constant was explored and illustrated in figure 5(a). According to the measurement results for different modulation indexes, by changing the index, the stimulation profile can be steered  $\pm 20$  mm from the centroid of the coil locations. Also, different combinations of the modulation index (instead of keeping one fixed and sweeping the other) can generate different E-field profiles.





Three examples of monophasic PWM-stimuli generated by the implemented magnetic pulse generator are shown in figures 5(b)–(d), as well as the measured E-field at the center and  $\pm 20$  mm away from the center, to test the efficiency of the proposed system (i)–(iii).

The coil voltages and currents were measured using a high-voltage differential probe (TA044, PICO TECHNOLOGY, UK) and a Rogowski current probe (I6000S FLEX-24, Fluke, USA), respectively. The peak coil current and delivered energy were measured to be 6 kA and 250 J, respectively. The behavior of the nerve tissue in the presence of an external E-field is modeled with a passive RC filter with a time constant of  $150 \mu\text{s}$ , as an accepted model for magnetic neuron stimulation [17, 33]. The conclusion is that changing the modulation index shifts the activation site.

### 3.1. Generation of conventional and user-defined stimuli

Using the concept of PWM and approximating a pulse waveform with this method, enables the synthesis

of any arbitrary pulse shapes, including conventional ones, and any combination of them into rapid pulse bursts in each channel. As shown in figure 6, the proposed pTMS2 device can generate a double pulse and triple (called polyphasic) or a single pulse (figures 5(b)–(d)), in the form of biphasic and monophasic waves. The achievable pulse frequency starts at 2 kHz and can be increased up to 5 kHz.

To enable further research on monophasic and biphasic rTMS methods, the pTMS2 device can generate high-frequency protocols with monophasic and biphasic or polyphasic stimulus shapes and repetition rates of up to 1 kHz (with an interstimulus interval of 1 ms). The energy recycling and the efficient modulation technique in this technology enable the generation of programmable and rapid stimulus sequences. In contrast to the previous TMS equipment, for which conventionally the output of several TMS devices must be combined, a single pTMS machine can generate and deliver a monophasic stimulus every 1 ms. Additionally, not all four waveforms must necessarily

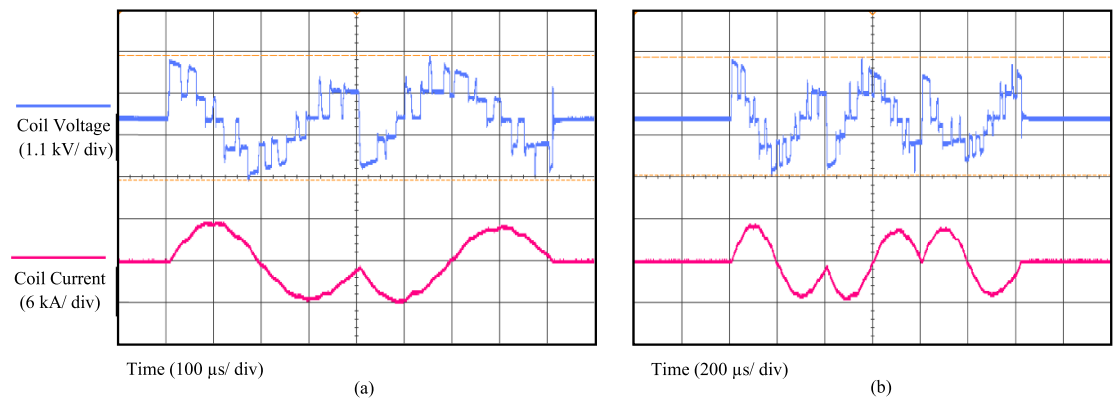


**Figure 6.** The measured waveform of the coil voltage and current for (a) double 2.5 kHz cosine stimuli where the two pulses have a phase difference of  $\pi$  radians and (b) triple 2.5 kHz cosine pulses with different phases.

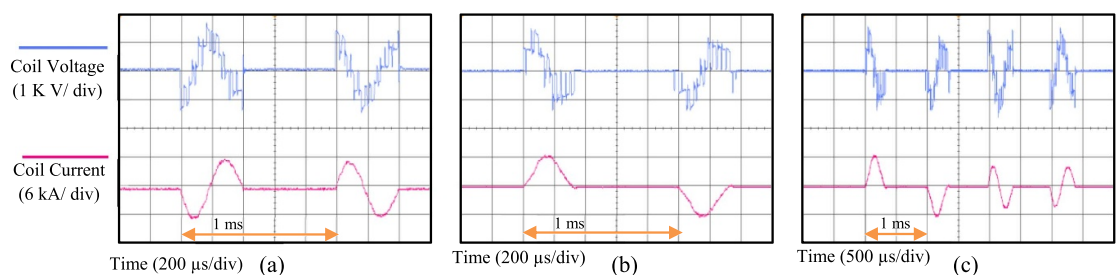


**Figure 7.** The measured waveforms for three different rapid TMS protocols to show the flexibility and ability to generate arbitrary pulse waveform in the burst: Coil voltage and current for (a) two 2.5 kHz cosine pulses with a 1 ms interval, where the two pulses have a phase difference of  $\pi$  radians. (b) Two 2.5 kHz sine pulses with a 1 ms interval, where the two pulses have a phase difference of  $\pi$  radians. (c) Four 2.5 kHz sine and cosine pulses with different phases. The time intervals are 1 ms, which is 1.5 times lower than the minimum interval used in the QPS protocol. For the voltage graphs, each square represents 1 kV, and for the current graph, each square corresponds to 6 kA.

be the same, as it is possible to program and change the stimulus waveform, and the phase of every single pulse.

Figure 7 illustrates examples of the proposed neurostimulator capability in generating rapid repetitive pulses. The measured parameters were set up for the generation of different sine and cosine stimuli with an interstimulus interval of 1 ms and different phases. Evidently, with a very short time interval, even lower than the required interval in the quadri-pulse stimulation (QPS) protocol, a relatively consistent stimulus can be delivered. In addition, the regeneration mode of the inverter recovers significant energy from the coil to the capacitors [17]. The maximum stimulation intensity of each pulse in 10 Hz rTMS, QPS, and intermittent theta-burst stimulation methods can be equal to the maximum system output (250 J), and for the continuous TBS the maximum available energy is 125 J. Therefore, in protocols such as QPS, there is no need to use several devices and a combining module.

The voltage decay for two pulses with an interval of 1 ms is about 5%. The use of pulse capacitors with much higher capacity than the conventional resonant-based circuit (5 mF for each channel

compared to 250  $\mu$ F in conventional TMS devices) is the main reason for low voltage decay. Because the maximum voltage is divided between two cells (i.e. each cell has a maximum voltage of 750 volts), capacitors with a lower voltage class but a larger capacity can be used. Also, the PI controller, by generating different trigger pulses in the burst, keeps the delivered energy almost constant. Therefore, for the same pulse width, by applying different on/off times of IGBT, in other words, optimum switch triggering to design pulse sequence for the TMS burst, the same effective energy will be delivered for each pulse of a burst. More details are available in the appendix (figure A2).

The TMS-induced E-fields generated by the pulses of (b) and (d) are shown as dashed and dash-dotted lines in (a), respectively. The E-field generated by the pulses of (c) is also presented in figure 4(C-iii). In (i) and (ii), for the voltage and current graphs, all amplitudes were normalized to the maximum. In all time axes, each square represents 100  $\mu$ s. All measurements were performed using a digital oscilloscope at a sampling rate of 500 MSa s<sup>-1</sup>. No bandwidth limitations or filters were employed to remove switching glitches/spikes.

## 4. Discussion

Power converters have been gaining popularity in TMS equipment owing to their potential to emulate arbitrary magnetic stimuli [16, 17]. The main reasons for the progress of the CHB are the reduction in power ratings and  $dv/dt$  across switches and the alleviation of the cost by reducing the power switch count. Owing to the modularity of CHB, it can be stacked for high-power magnetic stimulation applications. To generate a flexible magnetic pulse, CHB inverters must synthesize a staircase waveform using the PWM method. The PS-PWM method applied to CHB inverters enables highly effective overall switching frequencies for the generated stimulus, even with a low switching frequency of individual switch [25].

Nurmi *et al* demonstrated that there exists a trade-off between the induced E-field focality and the number of coils stacked on top of each other [34]. Optimal coil arrangements can provide wide control over the cortical region, whereas each coil requires a separate pulse generator and increases the system complexity. The use of two optimized coils on top of each other, and high-precision capacitive chargers proposed by Koponen *et al* [12], enables more focused targeting and shifting of the stimulated spot compared to this study. Because of the pulse generator circuit structure and elements used in it, such as capacitor chargers and relay-boards utilized for high-voltage sharing, it is not possible to charge/discharge the pulse capacitors quickly and this time may reach several seconds [35], so the stimulation location can be moved only in one direction and by increasing the voltage of the capacitors. In addition, the ability to change the stimulation type from real to sham has not been investigated in that structure.

TMS pulse generators whose pulse generation is based on the resonance; the pulse width of their output depends on the value of the inductance of the coil connected to it. Navarro de Lara *et al* also tried to minimize the dissimilarity of the three coils, but the remaining differences and mutual inductance caused the non-uniform pulse waveforms [13]. The proposed switching-based TMS design has a negligible waveform dependence on the coil inductance.

We anticipate that the presented TMS system will compensate for the patient's head movement during a stimulation sequence. The electronic stabilization of this method will be faster than the existing robot-assisted devices. The proposed system also allows changing the stimulation type from real to sham and vice versa, without changing the treatment coils themselves by modifying the modulation index parameters in software. This device also enables a closed-loop live target by gathering physiological signals during the stimulation session and deriving the coils from this data.

Using a switching-based CHB topology and the concept of a PWM can be an advantageous tool for setting up and enhancing such systems. Due to the high flexibility of stimulus waveform control by the PWM, stimulation paradigms can be optimized for more sophisticated functions and selective neuromodulation targets, and ultimately, expand the available parameter space to neurologists. Innovations in fundamental stimulation parameters will continue. Future methods of magnetic stimulation will aim for decreasing the variation in experimental studies and greater specificity. In the longer term, the researchers will have access to several safe and effective magnetic neurostimulator machines that provide specific, targeted, and adjustable treatment for most psychiatric and neurological disorders [36].

## 5. Limitations

As a limitation of the proposed system, owing to the physical distance of the coils, larger currents must be injected into the single coils to superimpose the fields of the two coils and achieve the stimulation profile of the Figure-of-eight coil, as shown in figure 4(iii). Also using a two-coil structure limits the continuous shifting of the peak E-field location. Changing the physical shape and number of coils, the number of winding turns, and stacking can help to adjust the location of the induced E-field and orientation more precisely on the cortex, although it will increase the complexity of the system. However, the introduced CHB topology and the concept of modulation index will compensate for the problem of delays of milliseconds.

The sham TMS technique introduced in this work and other studies [9, 10] would create the same subjective somatic scalp and facial muscles sensation during sham stimulation, on the other hand, the off-target stimulation may activate the premotor cortex. Therefore, the placebo protocol generated by this method can be considered as an active control condition.

From an economic point of view, switching-based systems generally require a higher cost to implement power electronic circuits (especially IGBTs), compared to resonant-based systems (Thyristors) [37].

## 6. Conclusion

The present neurostimulator establishes the unique potential of CHB inverter topologies to generate an arbitrary magnetic stimulus. The modular property of this inverter enables the improvement of the neuromodulation waveform by cascading H-bridges. The proposed pulse generator along with novel coil suggests the possibility of 'live steering' of stimulation type and spot without having to physically move the

coils themselves by modifying the effective intensity delivered to a fixed set of coils, as an example the coil can be driven in-phase to implement sham stimulation.

## Data availability statement

The data that support the findings of this study are available upon reasonable request from the authors.

## Acknowledgments

The authors would like to thank Magstim Company Ltd (UK) and Mark Phillips for construction, providing the stimulation coil, and valuable guidance on design considerations.

## Conflict of interest

All authors declare that they have no conflicts of interest or financial conflicts to disclose.

## ORCID iD

Majid Memarian Sorkhabi  <https://orcid.org/0000-0002-9449-0738>

## References

- [1] Edelman B J *et al* 2015 Systems neuroengineering: understanding and interacting with the brain *Engineering* **1** 292–308
- [2] Lefaucheur J P *et al* 2014 Evidence-based guidelines on the therapeutic use of repetitive transcranial magnetic stimulation (rTMS) *Clin. Neurophysiol.* **125** 2150–206
- [3] Zhang Y *et al* 2020 Identification of psychiatric disorder subtypes from functional connectivity patterns in resting-state electroencephalography *Nat. Biomed. Eng.* **5** 309–23
- [4] Epstein C M 2008 Electromagnetism *The Oxford Handbook of Transcranial Stimulation* ed E Wassermann, C Epstein, U Ziemann, V Walsh, T Paus and S Lisanby (Oxford: Oxford University Press) pp 3–5
- [5] MAGSTIM Company 2009 *Magstim Rapid 2 P/N 3576–23-09 Operating Manual* (Whitland: The MAGSTIM Company LTD)
- [6] Robertson E M, Théoret H and Pascual-Leone A 2003 Studies in cognition: the problems solved and created by transcranial magnetic stimulation *J. Cognit. Neurosci.* **15** 948–60
- [7] Grasin E, Loginov I, Masliukova A and Smirnov N 2019 Realistic sham TMS *Brain Stimul.* **12** 418
- [8] Mennemeier M *et al* 2009 Sham transcranial magnetic stimulation using electrical stimulation of the scalp *Brain Stimul.* **2** 168–73
- [9] Hoeft F *et al* 2008 Electronically switchable sham transcranial magnetic stimulation (TMS) system *PLoS One* **3** 1–10
- [10] Ruohonen J *et al* 2000 Coil design for real and sham transcranial magnetic stimulation *IEEE Trans. Biomed. Eng.* **47** 145–8
- [11] Kantelhardt S *et al* 2010 Robot-assisted image-guided transcranial magnetic stimulation for somatotopic mapping of the motor cortex: a clinical pilot study *Acta Neurochir.* **152** 333–43
- [12] Koponen L M, Nieminen J O and Ilmoniemi R J 2018 Multi-locus transcranial magnetic stimulation—theory and implementation *Brain Stimul.* **11** 849–55
- [13] Navarro de Lara L I *et al* 2021 A 3-axis coil design for multichannel TMS arrays *NeuroImage* **224** 117355
- [14] Peterchev A V, Jalinous R and Lisanby S H 2008 A transcranial magnetic stimulator inducing near-rectangular pulses with controllable pulse width (cTMS) *IEEE Trans. Biomed. Eng.* **55** 257–66
- [15] Peterchev A V, Murphy D L and Lisanby S H 2011 Repetitive transcranial magnetic stimulator with controllable pulse parameters *J. Neural Eng.* **8** 036016
- [16] Peterchev A V, D'Ostilio K, Rothwell J C and Murphy D L 2014 Controllable pulse parameter transcranial magnetic stimulator with enhanced circuit topology and pulse shaping *J. Neural Eng.* **22** 1–12
- [17] Memarian Sorkhabi M *et al* 2020 Programmable transcranial magnetic stimulation- a modulation approach for the generation of controllable magnetic stimuli *IEEE Trans. Biomed. Eng.* **68** 1847–58
- [18] Wendt K, Memarian Sorkhabi M, O'Shea J, Cagnan H and Denison T 2021 Comparison between the modelled response of primary motor cortex neurons to pulse-width modulated and conventional TMS stimuli *43rd Annual Int. Conf. of the IEEE Engineering in Medicine & Biology Society (EMBC) (Mexico)* (<https://doi.org/10.1109/EMBC46164.2021.9629605>)
- [19] Memarian Sorkhabi M *et al* 2021 A digital transcranial magnetic stimulator for generating arbitrary pulse-shapes and patterns *Brain Stimul.* **14** 1613–4
- [20] Memarian Sorkhabi M, Wendt K, Wilson M T and Denison T 2021 Estimation of the motor threshold for near-rectangular stimuli using the hodgkin–huxley model *Comput. Intell. Neurosci.* **2021** 1–10
- [21] Muhammad R H 2004 *Power Electronic Circuits, Devices, and Applications* (Upper Saddle River, NJ: University of West Florida, Pearson Prentice Hall)
- [22] Leon J I *et al* 2016 The essential role and the continuous evolution of modulation techniques for voltage-source inverters in the past, present, and future power electronics *IEEE Trans. Ind. Electron.* **63** 2688–701
- [23] Franquelo L G, Rodriguez J, Leon J I and Kouro S 2008 The age of multilevel converters arrives *IEEE Ind. Electron. Mag.* **2** 28–39
- [24] Marquez A, Leon J I, Vazquez S, Portillo R, Franquelo L G, Freire E and Kouro S 2017 Variable-angle phase-shifted PWM for multilevel three-cell cascaded H-bridge converters *IEEE Trans. Ind. Electron.* **64** 3619–28
- [25] da Silva E R C *et al* 2011 Pulse width modulation strategies *IEEE Ind. Electron. Mag.* **5** 37–45
- [26] Srndovic M *et al* 2018 Simultaneous selective harmonic elimination and THD minimization for a single-phase multilevel inverter with staircase modulation *IEEE Trans. Ind. Appl.* **54** 1532–41
- [27] Barbie E *et al* 2020 Closed-form analytic expression of total harmonic distortion in single-phase multilevel inverters with staircase modulation *IEEE Trans. Ind. Electron.* **67** 5213–6
- [28] Zheng Y *et al* 2021 Research on DC protection strategy in multi-terminal hybrid HVDC system *Engineering* **7** 1064–75
- [29] Memarian Sorkhabi M, Wendt K, Rogers D and Denison T 2021 Paralleling insulated-gate bipolar transistors in the H-bridge structure to reduce current stress *SN Appl. Sci.* **3** 1–8
- [30] Wang L *et al* 2015 PID and predictive control of electrical drives and power converters using MATLAB/Simulink (New York: Wiley)
- [31] Wu B and Narimani M 2017 Two-level voltage source inverter *High-Power Converters and AC Drives* (Piscataway, NJ: Wiley-IEEE Press) pp 93–117
- [32] Sahoo B, Routray S K and Rout P K 2019 Repetitive control and cascaded multilevel inverter with integrated hybrid active filter capability for wind energy conversion system *Int. J. Eng. Sci. Technol.* **22** 811–26

- [33] Barker A, Garnham C and Freeston I 1991 Magnetic nerve stimulation: the effect of waveform on efficiency, determination of neural membrane time constants and the measurement of stimulator output *Electroencephalogr. Clin. Neurophysiol. Suppl.* **43** 227–37
- [34] Nurmi S, Karttunen J, Souza V H, Ilmoniemi R J and Nieminen J O 2021 Trade-off between stimulation focality and the number of coils in multi-locus transcranial magnetic stimulation *J. Neural Eng.* **18** 066003
- [35] Sinisalo H, Nieminen J and Ilmoniemi R 2021 Waveform simulation and pulse-width-modulation approximations with multi-locus tms *Brain Stimul.* **14** 1634
- [36] Denison T and Morrell M J 2022 Neuromodulation in 2035: the neurology future forecasting series *Neurology* **98** 65–72
- [37] Sorkhabi M M *et al* 2021 Design analysis and circuit topology optimization for programmable magnetic neurostimulator *43rd Annual Int. Conf. IEEE Engineering in Medicine & Biology Society (EMBC) (Mexico)* (<https://doi.org/10.1109/EMBC46164.2021.9630915>)